Electrochimica Acta 245 (2017) 79–87

Contents lists available at ScienceDirect

Electrochimica Acta

journal homepage: www.elsevier.com/locate/electacta

Bidimensional Spectroelectrochemistry: application of a new device in the study of a *o*-vanillin-copper(II) complex

D. Izquierdo[a], V. Ferraresi-Curotto[b], A. Heras[a], R. Pis-Diez[b], A.C. Gonzalez-Baro[b], A. Colina[a,*]

[a] Department of Chemistry, Universidad de Burgos, Pza. Misael Bañuelos s/n, E-09001 Burgos, Spain
[b] CEQUINOR (CONICET, UNLP), CC 962, B1900AVV La Plata, Argentina

ARTICLE INFO

Article history:
Received 2 February 2017
Received in revised form 16 May 2017
Accepted 16 May 2017
Available online 18 May 2017

Keywords:
spectroelectrochemistry
electrochemistry
copper
reaction mechanism

ABSTRACT

A new bidimensional spectroelectrochemistry setup for UV-Vis absorption measurements has been developed. The new device has been used to follow electrochemical reactions using two different arrangements: 1) a near-normal configuration that supplies information about the processes taking place both on the electrode surface and in the solution adjacent to it, and 2) a long-optical-pathway configuration based on a mobile slit that controls the position of a light beam passing parallel and adjacent to the electrode surface providing information only about the processes taking place in solution during the electrochemical reaction. The new setup has been validated using *o*-tolidine, a typical reference system for spectroelectrochemistry. The electrochemical mechanism of oxidation/reduction of $Cu(o\text{-}Va)_2(H_2O)_2$ complex (*o*-Va = *o*-Vanillin = 2-hydroxy-3-methoxybenzaldehyde) has been studied using bidimensional UV-Vis absorption spectroelectrochemistry. This Cu(II) complex exhibits antimutagenic, anticarcinogenic and superoxide dismutase mimic properties.

1. Introduction

Spectroelectrochemistry (SEC) is a powerful instrumental technique that combines two classical analytical techniques, such as electrochemistry and spectroscopy, to obtain *in situ* chemical information [1–6] about the reactions taking place during an electrochemical experiment. Usually, the electrochemical technique controls the chemical process, while spectroscopy provides molecular information about chemical compounds involved in the process, being complementary to the electrochemical information. Since 1964, when Kuwana proposed this technique [7], many approaches using different experimental setups [8–14] have been proposed to improve the quality and significance of the spectroelectrochemical experiments, trying to shed more light on the processes involved in the electrochemical reactions.

UV-Vis absorption spectroelectrochemistry can be performed in two different optical configurations, taking into account the position of the light beam with respect to the working electrode: normal [15,16] and parallel [17–19] arrangement. On the one hand, in normal configuration the light beam goes through the diffusion layer perpendicularly to the working electrode surface. In this case, a transmission [20,21] or a reflectance [22,23] experimental setup can be used. On the other hand, in parallel configuration, also known as long-optical-pathway configuration, the light beam passes parallel to the electrode surface, with the light beam sampling the adjacent solution to the electrode surface [19,24,25]. Each configuration provides different type of information about the processes occurring at the electrode surface. Normal configuration mainly supplies information about the whole diffusion layer, including the compounds adsorbed or crystalized on the electrode surface, but also a small contribution of species in the solution near the electrode can be obtained. However, parallel configuration only provides information about the processes occurring in the solution close to the electrode. Besides, this second arrangement guarantees a longer optical pathway than in normal configuration. The main drawback of parallel configuration is the lack of sensitivity to adsorption/crystallization phenomena taking place on the electrode surface.

Usually, only one of these configurations is chosen depending on the chemical problem, but in many cases both kind of information are necessary to fully understand the studied chemical system. In this respect, bidimensional spectroelectrochemistry (BSEC) [26] allows us to perform simultaneously measurements in the two configurations, obtaining in only one experiment a more

* Corresponding author.
E-mail address: acolina@ubu.es (A. Colina).

http://dx.doi.org/10.1016/j.electacta.2017.05.105
0013-4686/

complete picture on the electrode processes. The main disadvantage of BSEC is the complexity of the spectroelectrochemical cells to get reproducible and good enough experimental results. Recently this problem has been minimized using optical fibers, simplifying the correct alignment of the light beam and improving the reproducibility of the experiment [27]. In this work, another setup with specific improvements is proposed for BSEC. On one hand we use a simple three electrode system placed in a spectrophotometric cuvette together with a reflection probe for normal configuration measurements. On the other, we use piezoelectric positioners to control the position of a slit that allows us to place the light beam adjacent to the electrode at controlled distances. Thus, although parallel beam alignment is usually very complex and troublesome, by using this new approach, previously tested with liquid/liquid interfaces [20], the experiments can be performed in a very simple and easy way.

Firstly, *o*-tolidine has been selected as reference system to prove the good performance of this new spectroelectrochemical setup [26,28,29]. Finally, BSEC has been used to study the electrochemical mechanism of reaction of, $[Cu(o\text{-}Va)_2(H_2O)_2]$ complex (*o*-Va = *o*-vanillin = 2-hydroxy-3-methoxybenzaldehyde).

Copper can be coordinated by ligands with therapeutic properties, often with a synergic effect on the activity, as the metal center improves the mobility and bio availability of the agent. The studied compound, Cu-*o*-Va is an antimutagenic, anticarcinogenic agent and exhibits superoxide dismutase (SOD) mimic properties. In particular, the ligand *o*-vanillin, as other related hydroxyaldehydes, has demonstrated antimutagenic and carcinogenesis inhibitory activities and is also an antioxidant agent and scavenger of free radicals. It has been employed in the syntheses of many active poly-functional ligands, including those belonging to the Schiff Bases family, that form many active copper complexes, among other metals.

In this work we report the usefulness of the new BSEC spectroelectrochemical setup proposed to understand the complex electrochemistry of $[Cu(o\text{-}Va)_2(H_2O)_2]$ in dimethylsulfoxide solution.

2. Experimental

2.1. Chemicals and Materials

o-Tolidine (Sigma-Aldrich), *o*-vanillin (*o*-Va, Sigma-Aldrich), tetrabuthylammonium hexafluorophosphate ($TBAPF_6$, Merck), dimethylsulfoxide (DMSO, Sigma-Aldrich), acetic acid (HAc, Acros) and perchloric acid ($HClO_4$, Acros) are analytical grade and used as received without further purification. $[Cu(o\text{-}Va)_2(H_2O)_2]$ was prepared according to a reported synthesis procedure [30,31] from equimolar amounts of *o*-Va and $Cu(CH_3COO)_2$. *o*-Va was dissolved in methanol and dropwise added, under continuous stirring to a 2:1 methanol:water solution of $Cu(CH_3COO)_2$. The mixture was stirred for 30 min, and the left to stand at room temperature until bright yellowish green monocrystals were obtained. Deionized water with a resistivity of 18 MΩ cm (Milli-Q purification system, Millipore), is used to prepare aqueous solutions. Analytical grade DMSO (Fisher Chemical) was used for prepared nonaqueous solutions. For safety considerations, all handling and processing were performed carefully particularly when *o*-tolidine and DMSO was used.

2.2. Instrumentation

A new experimental setup (Fig. 1 and Figure SI1) has been developed to perform BSEC experiments using a mobile slit to locate the desired position of the light beam in the parallel arrangement. The experimental setup used for BSEC measurements to control the

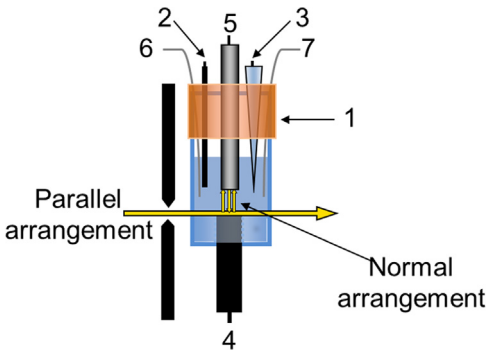

Fig. 1. Scheme of the spectroelectrochemical cell. (1) Suba-Seal septa, (2) auxiliary electrode, (3) reference electrode, (4) working electrode, (5) reflection probe, (6) N_2 inlet, (7) N_2 outlet.

motion of the slit are based on previous works [18], where a detailed description of the device can be found. In the present work, the previous liquid/liquid interface is replaced by a solid electrode. The mobile slit device consists of a rigid block supporting the slit and the lenses, attached to the positioner in order to transmit the motorized actuator movement to the whole block. The slit is located between two collimating lenses with fitted optical fibers. Normal arrangement is based on a near-normal incident reflection spectroelectrochemical configuration (NNIRS) [32,33]. Spectroelectrochemical experiments were carried out using a PGSTAT 302N potentiostat (Eco Chemie B.V) coupled to two QE65000 Spectrometers (Ocean Optics) one for each configuration. The potentiostat and the two spectrometers were exactly synchronized with an external trigger. The common end of a 200-μm bifurcated fiber (Ocean Optics) was connected to a DH-2000 Deuterium-halogen light source (Ocean Optics). One of the fibers end of the bifurcated fiber is attached to a 450-μm diameter optical fiber (Ocean Optics) and used for parallel configuration measurements, while the other fiber end is connected to a reflection probe (FCR-7UV200-2-1.5 × 1SR, Avantes) to perform normal configuration measurements. The reflection probe is connected to the other spectrometer. The 450-μm diameter optical fiber in parallel configuration leads the light beam from the light source to a collimating lens that is fixed to the holder before crossing the solution. The light beam after sampling the solution in parallel configuration is collected by a collimating lens and is conducted to the spectrometer using a 450-μm diameter optical fiber (Ocean Optics).

The last and central part of this setup is the spectroelectrochemical cell (Fig. 1). It consist of a three-electrode system with a glassy carbon disk as working electrode (WE), a platinum wire as auxiliary electrode (AE) and a home-made Ag/AgCl/3 M KCl reference electrode (RE). The three-electrode system is placed in a modified commercial quartz spectrophotometric cuvette 110-QS (Hellma) to properly perform simultaneously the experiment in the two spectroscopic configurations. Thus, the bottom part of the quartz cuvette was cut to fill it with the corresponding solution and to place the reflection probe and the reference and auxiliary electrodes. The WE was placed in the cuvette hole usually used to fill the cuvette, sealing the electrode with Teflon tape to avoid any leakage of the solution when the cuvette is placed in an inverted position during a BSEC experiment. Next, a Suba-Seal septa with five drilled holes is used to close the upper part of cuvette and to properly fix the reference and the auxiliary electrode, the reflection probe, the nitrogen inlet and outlet, and to avoid any interference with the light beam in parallel configuration.

All the experiments were performed in a semiinfinite diffusion regime. Actually, this is the most used diffusion regime in electrochemistry. Although thin-layer cells are commonly used in spectroelectrochemistry to obtain formal potentials and number

of electrons of redox couples, time resolved spectroelectrochemistry is more useful to follow diffusive processes, providing molecular information on the reactants and/or products involved in the electron transfer process.

Absorbance data from all spectroelectrochemical experiments were calculated taking as reference spectrum the one at the starting potential of each individual experiment.

Mass spectrometry experiments were carried out using a Micromass AutoSpec (WATERS).

2.3. Computational methods

The geometry of all the species under study were optimized using the B3LYP hybrid density functional [34,35]. The cc-pVDZ [36] basis set was used for H and C, whereas the aug-cc-pVDZ [36,37] basis set was utilized for O. On the other hand, the cc-pVDZ-PP [38,39] basis set, which includes a pseudopotential to represent inner electrons up to the 2p sub-shell, was used for Cu.

To facilitate the comparison of theoretical results with experimental data, geometry optimizations and calculation of properties were performed including solvent effects (DMSO) through the Polarizable Continuum Model [40,41].

The Hessian matrix of the total energy with respect to the nuclear coordinates of every molecule was calculated at the same level of theory and was diagonalized to verify whether they are local minima or saddle points on the corresponding potential energy surfaces.

The electronic spectra of all the species in DMSO were calculated using the time dependent density functional theory (TDDFT) [42]. All the calculations were carried out with the Gaussian 09 package [43].

3. Results and discussion

3.1. Validation

The experimental setup for BSEC measurements (Fig. 1 and Figure SI1) was validated using *o*-tolidine. This well-known reference system for spectroelectrochemistry was chosen because it exhibits a fast two electron transfer and a large molar absorption coefficient in water, $\varepsilon = 60670\ M^{-1}\ cm^{-1}$ at 438 nm [44]. Fig. 2 shows a validation experiment carried out by cyclic voltammetry, scanning the potential between +0.45 V and +0.80 V at $0.005\ V\ s^{-1}$ in a 10^{-4} M *o*-tolidine, 0.5 M HAc and 1 M $HClO_4$ aqueous solution. Fig. 2.a, shows the corresponding cyclic voltammogram (CV) obtained during electroxidation of *o*-tolidine, with an anodic peak emerging at +0.645 V that is related to the electrogeneration of *o*-tolidinium cation, and a reversible cathodic peak at +0.610 V that is related to the reduction of this cation to *o*-tolidine. The evolution of the spectra with time (potential) in normal and parallel configuration, obtained during the electrochemical reaction, is shown in the supporting information (Figures SI2.a, and SI2.b). In both figures the corresponding contour plots of these 3D images are overlapped to a better understanding of absorbance changes. In the two configurations, a characteristic maximum of absorbance at 438 nm due to the generation of *o*-tolidinium cation can be observed. In the backward scan, this band decreases in intensity due to the regeneration of *o*-tolidine. The main differences between the spectra in the two spectrophotometric arrangements is the absorbance value, higher in parallel configuration due to the longer optical path-way compared with that in normal configuration. This fact makes more sensitive the parallel arrangement for studying electrochemical processes in which only soluble compounds are involved. Fig. 2.b and 2.c shows the voltabsorptograms (VA) at 438 nm obtained in normal and parallel configuration, respectively. VA in normal configuration at the maximum of

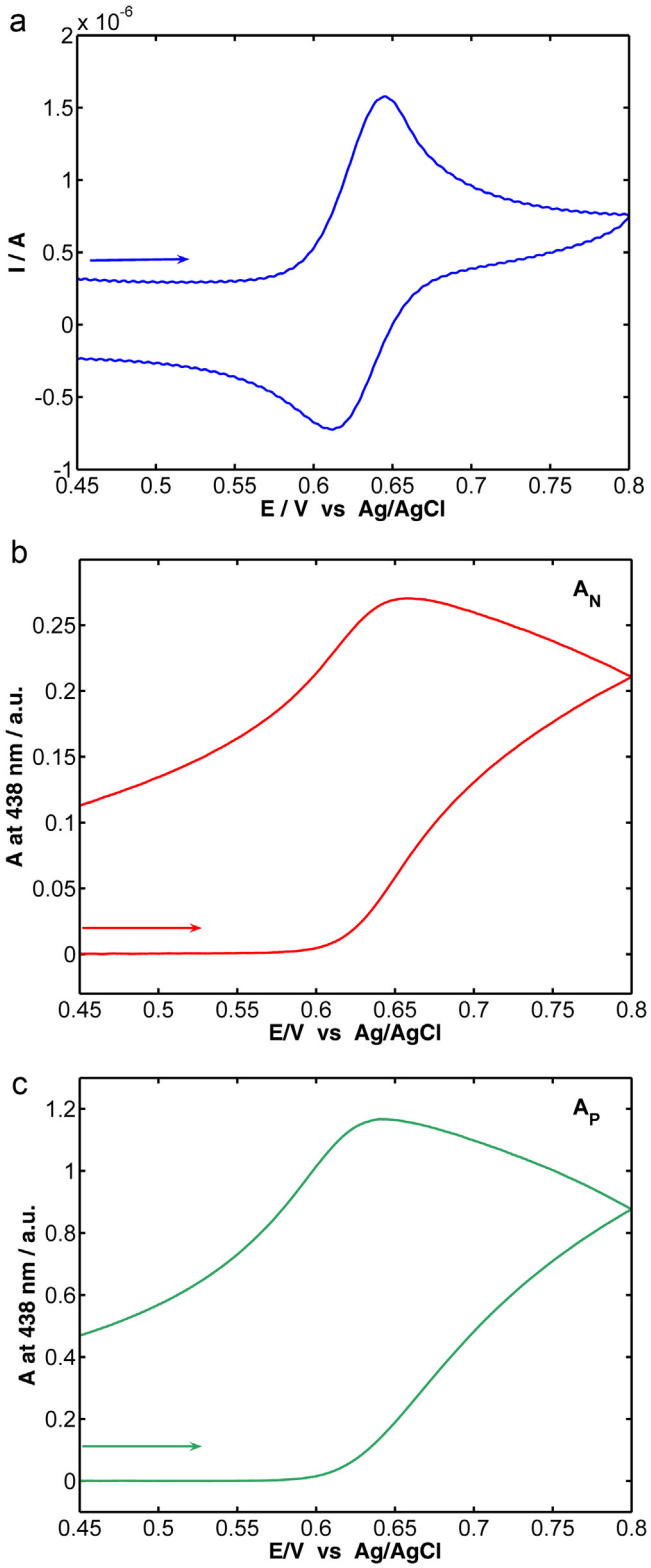

Fig. 2. (a) Cyclic voltammogram, (b) cyclic voltabsorptogram in normal configuration at 438 nm, (c) cyclic voltabsorptogram in parallel configuration at 438 nm. Potential was scanned from +0.45 V to +0.80 V at $0.005\ V\ s^{-1}$ in a 10^{-4} M *o*-tolidine, 0.5 M HAc and 1 M $HClO_4$ aqueous solution.

absorption, Fig. 2.b, shows an increase of absorbance during the oxidation of *o*-tolidine due to the generation of *o*-tolidinium cation, and the subsequent decrease during the reversible reduction of the cation to *o*-tolidine .On the other hand, VA at 438 nm in parallel

configuration, Fig. 2.c, shows the same behavior but the amount of *o*-tolidine that is observed is much higher because of the longer optical-pathway. These results indicate the suitable implementation of parallel configuration in the spectroelectrochemical setup proposed.

3.2. Study the electrochemical mechanism of oxidation/reduction of Cu-o-Va

The behavior of the optical and electrical responses, shown above, indicates that high quality spectroelectrochemical measurements can be performed using this new BSEC setup. The electrochemical reaction mechanism of the Cu-*o*-Va is much more complex than that of *o*-tolidine, and this BSEC setup would help to shed more light on this reaction mechanism. For this purpose, cyclic voltammetry experiments were performed using a wide potential window in order to obtain a whole picture of the redox processes in which Cu-*o*-Va is involved. Solutions were accurately purged by passing a dry N_2 stream for 300 s before each experiment. Based on previous experiments, a potential window from −0.70 to +1.30 V was selected, fixing the starting and ending potential at 0.00 V where different electrochemical process took place. Using this potential window, two voltammetric cycles at 0.010 V s^{-1} were performed in a 10^{-3} M Cu-*o*-Va and 0.1 M $TBAPF_6$ DMSO solution. The spectroelectrochemistry responses are summarized in Fig. 3.

The CV of the first potential cycle (Fig. 3.a, blue line) exhibits an ill-defined reduction process around −0.50 V and a clear irreversible oxidation peak at +1.18 V. Spectroscopic results provide complementary and very suitable information about the processes taking place during this reaction. Comparison of full spectra, shown as contour plots in normal and parallel configuration, Figs. 3.b and 3.c respectively, indicates a different behaviour in the two configurations. A representation of the current respect to time/potential has been added at the left of the contour plot for an easier understanding of the absorption bands. In the first cycle, the spectra in normal configuration (Fig. 3.b, blue line in E-I plot) show two main absorption bands. The first one band is observed at 475 nm around −0.70 V and the second one emerges at 510 nm around +1.30 V. Analysing the spectra in parallel configuration obtained during the first potential cycle (Fig. 3.c, blue line in E-I plot), only the absorption band at 510 nm is observed. Fig. 3.d shows the VA at 510 nm obtained during the first cycle for both configurations. As can be observed, during the reduction process, the absorbance in A_N at 510 nm is significantly higher than the absorbance in A_P at the same wavelength although the optical path-length is longer in parallel than in normal configuration. Thus, different processes are observed in the two configurations. These differences can be explained in terms of an electrodeposition process taking place on the electrode surface. Therefore, we can conclude that during the cathodic scan at potentials lower than −0.45 V, the reduction from Cu(II) to Cu(0) is taking place, while

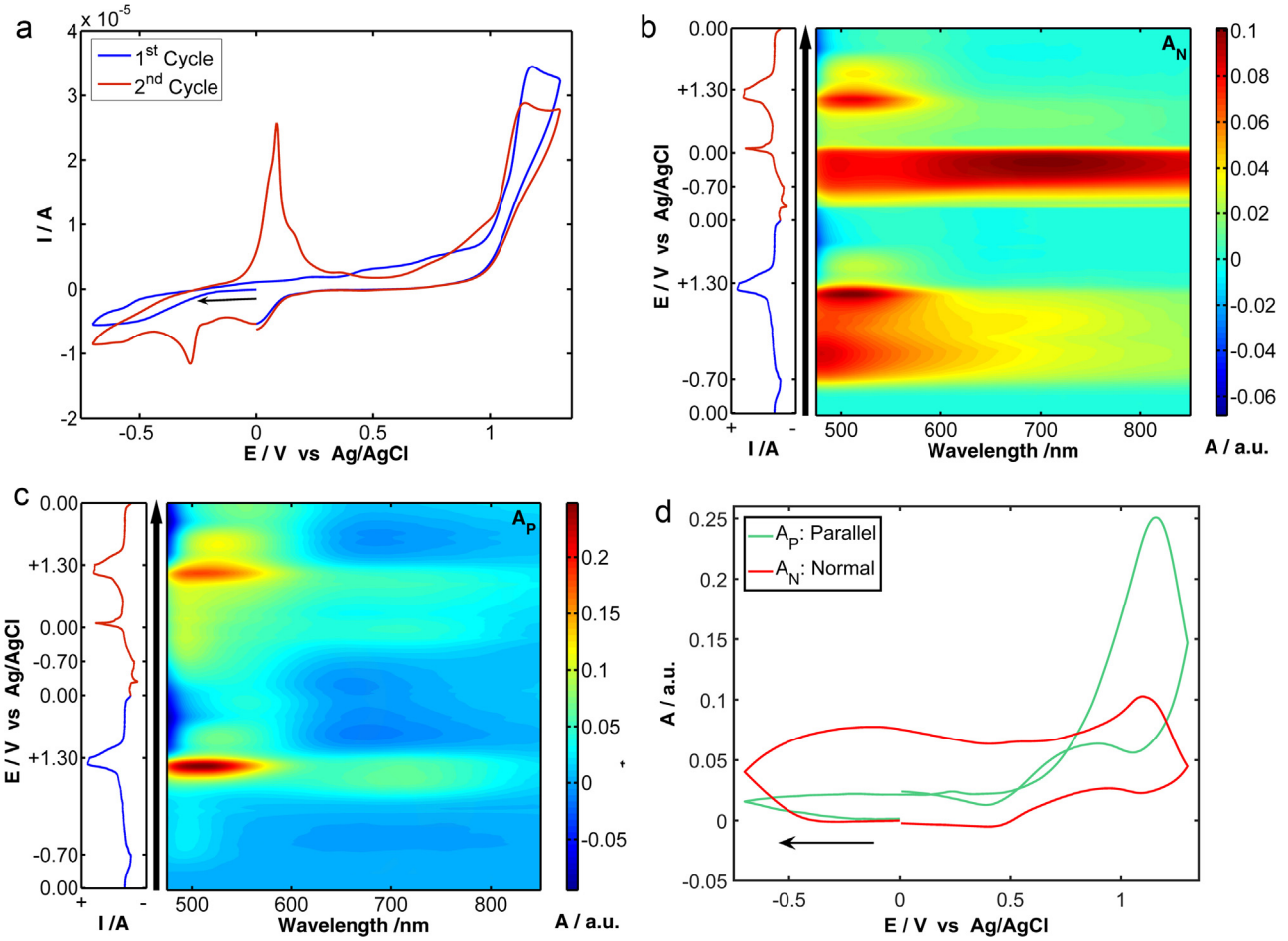

Fig. 3. (a) Cyclic voltammogram and contour plots of absorbance evolution with time (potential) in (b) normal and (c) parallel configuration during the two potential cycles. For a better understanding of the contour plots, the corresponding 3D plots of absorbance evolution with potential are shown in the supporting info, Figure SI3. (d) Voltabsorptograms at 510 nm in normal and parallel configuration during the first potential cycle. Two potential cycles from 0.00 V to −0.70 V and back to +1.30 V, ending the experiment at 0.00 V, scanning the potential at 0.01 V s^{-1}. Experiment performed in 10^{-3} M Cu-*o*-Va and 0.1 M $TBAPF_6$ DMSO solution.

the reduction to Cu(I) is not observed because no absorption bands are observed in parallel configuration related to these processes. If the reduction reaction took place only in solution, A_P should be higher than A_N because of the difference of the optical pathways.

During the anodic scan, the CV (Fig. 3.a, blue line) does not show any defined oxidation peak due to the oxidation of Cu(0), but A_N around 475 nm in the contour plot (Fig. 3.b) shows a very small decrease of A_N at 0.00 V that could be related to a very small oxidation of Cu(0). At more positive potentials, +1.18 V, an irreversible peak is observed both in the CV and the VA at 510 nm (blue line in Fig. 3.a and Fig. 3.d), due to the oxidation of the Cu-*o*-Va. In this case, A_P at 510 nm is higher than A_N (Fig. 3.d) indicating that this process is taking place only in solution. A similar behaviour is observed in a pure *o*-Va solution, ascribing this oxidation peak to the oxidation of the *o*-Va ligand, as has been reported in previous works [45]. The calculated spectrum of the oxidized form of the free ligand *o*-Va shows a band at 520 nm, similar to that obtained experimentally, indicating a good correlation between experimental and theoretical data. Finally, it should be mentioned that at the end of the first potential scan, a reduction peak is observed around 0.00 V in the voltammogram, but any change in the spectral signals is observed.

Inspecting spectroelectrochemical responses during the second potential cycle a more complete map of the electrochemical reaction can be obtained. Two additional reduction peaks are observed during the second scan in the CV (Fig. 3.a, red line). The first one at 0.00 V and the second one at −0.30 V, together with the ill-defined peak around −0.50 V, previously observed in the first cycle. During this second cycle, in the backward scan the reoxidation of Cu(0) at +0.05 V is clearly detected together with a post-peak shoulder that could be related to the reduction peak appearing at 0.00 V. Also, the oxidation peak of the *o*-Va ligand of the copper complex is observed in the two cycles. Moreover, in the second cycle contour plots of spectral responses (Figs. 3.b and 3.c) show some relevant changes compared with the first cycle. The more significant change is appreciated in spectra evolution in normal configuration (Fig. 3.b) where a very broad band around 720 nm is observed at potentials lower than 0.00 V. This absorption band disappears at potential higher than 0.00 V. However, this absorption band at 720 nm is not observed in the spectra registered in parallel configuration. Therefore, this broad band peaking at 720 nm has to be ascribed to the generation of Cu(0) on the electrode, with the metal being subsequently redissolved, as can be deduced from the sharp peak in the voltammogram at +0.05 V.

Consequently, from the spectra in normal configuration we can deduce that two different processes occur on the electrode surface. First, the deposition of nuclei of Cu(0) on the glassy carbon electrode during the first cycle (band at 475 nm, around −0.50 V), and next, during the second cycle, the deposition of Cu(0) on Cu(0) nuclei yielding a Cu(0) film (band at 720 nm). On the other hand, in parallel configuration only the oxidation in solution of the ligand of the Cu-*o*-Va complex is observed (band at 510 nm, around +1.10 V). It is noteworthy that there is not any clear absorption band either in normal or parallel configuration related to the reduction peak appreciated around 0.00 V.

In the previous experiment the concentration of Cu-*o*-Va was too high to observe spectral changes below 475 nm, therefore we decide to decrease this value to $5{\cdot}10^{-4}$ M. In addition, the preceding study was performed starting the experiment through the cathodic direction. To determine if this experimental condition controls the spectroelectrochemical behaviour explained above, now we present a similar experiment but scanning first the potential through anodic values. Thus, we carried out a cyclic voltammetry in a DMSO solution $5{\cdot}10^{-4}$ M Cu-*o*-Va and 0.1 M $TBAPF_6$, scanning the potential at 0.01 V s^{-1} from +0.60 V to +1.20 V and back to −0.70 V, finishing at the starting potential, +0.60 V.

Fig. 4 shows the three spectroelectrochemical responses obtained during this experiment. The CV (Fig. 4.a) in this case only shows the irreversible oxidation peak at +1.10 V, the reduction peak at 0.00 V, another ill-defined peak around −0.50 V and the oxidation peak at +0.05 V. As in the former experiment, the sharp stripping oxidation peak at +0.05 V is overlapped with a less

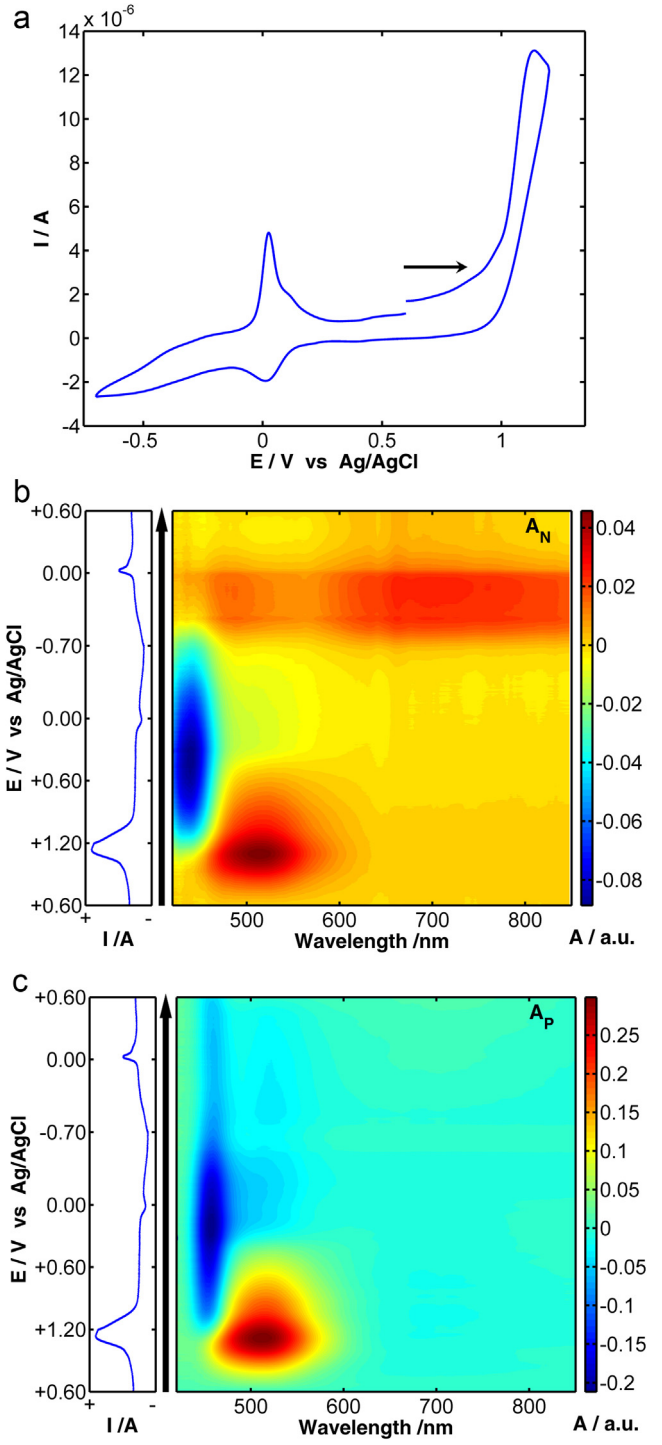

Fig. 4. (a) Cyclic voltammogram and contour plots of absorbance evolution with time (potential) in (b) normal and (c) parallel configuration. For a better understanding of the contour plots, the corresponding 3D plots of absorbance evolution with potential are shown in the supporting info, Figure SI4. One potential cycle from +0.60 V to +1.30 V and back to −0.70 V, ending the experiment at +0.60 V, scanning the potential at 0.01 V s^{-1}. Experiment performed in $5{\cdot}10^{-4}$ M Cu-*o*-Va and 0.1 M $TBAPF_6$ DMSO solution.

intense diffusive peak. The evolution of the spectra in normal configuration with the potential applied (Fig. 4.b) confirms that the copper complex is oxidized at +1.10 V, as can be deduced from the band evolving at 510 nm. Additionally, a narrow and well-defined absorption band emerges at 425 nm at potentials where no electrochemical reaction is taking place. This experimental result must be explained as a charge redistribution within the complex of the oxidized Cu-*o*-Va complex, as will be explained bellow, that is subsequently reduced at 0.00 V. Contour plot of spectra in parallel configuration (Fig. 4.c) confirms this hypothesis because both bands, 510 nm and 425 nm, are also observed indicating that both processes, oxidation of the complex and the following charge redistribution, take place in solution. The main difference appreciated between the two optical responses is observed in the cathodic region. As in the experiment shown in Fig. 4, the electrodeposition of Cu(0) is only observed in normal arrangement (Fig. 4.b), yielding a Cu(0) film on the electrode that is redissolved around +0.05 V, as evidenced by the sharp peak in the backward scan of the CV (Fig. 4.a).

The reduction peak at 0.00 V is attributed in the bibliography to a quasi-reversible electron transfer process [30] for the redox couple Cu^{II}/Cu^{I}. Joining this assignment to our results, we can suggest that the pristine Cu-*o*-Va complex can only be reduced directly to Cu(0) (first cycle in Fig. 4) that implies the breakdown of the complex. However, when the Cu-*o*-Va complex is oxidized, it takes place over the phenolic oxygen of the ligand. The new complex right after, can be reduced from Cu(II) to Cu(I). The absence of the reduction peak at −0.30 V in this experiment, indicates that the presence of this peak in the second cycle of the CV in the previous experiment (Fig. 3.a) should be related to the reduction of free Cu(II) generated during the reoxidation in this second scan of the Cu(0) nuclei, that were deposited in the first scan.

New cyclic voltammetric experiments with a more diluted solution were performed to demonstrate with certainty the reduction of the oxidized Cu(II)-complex to Cu(I)-complex. In this case, the experiment was done reaching a vertex potential in the cathodic direction where the generation of Cu(0) is avoided. Cyclic voltammetry experiments were carried out between −0.10 V and +1.25 V, potential window wide enough to promote the reduction from Cu(II) to Cu(I), but not to yield to Cu(0). The spectroelectrochemistry results of this experiment are summarized in Fig. 5. For comparison with the results shown above in Figs. 4 and 5, two experiments were performed, both working with 10^{-4} M Cu-*o*-Va and 0.1 M $TBAPF_6$ DMSO solutions, scanning the potential at 0.005 V s^{-1}. The first experiment starts through the cathodic direction (Figure SI3) while the second one is carried out through the anodic direction (Fig. 5). In the first case (Figure SI6), two consecutive scans were performed from +0.50 V to −0.10 V and back to +1.20 V, ending the experiment at the starting potential, +0.50 V. The first scan in the CV (Figure SI6) shows that during the cathodic scan the reduction of Cu(II) to Cu(I) does not occur, demonstrating, as it was stated above, that the Cu-*o*-Va complex is not reduced to Cu(I).

Fig. 5 shows the spectroelectrochemical responses obtained in the second experiment scanning the potential from +0.50 V to +1.20 V and back to −0.10 V, ending the experiment at the starting potential, +0.50 V. Both processes, the oxidation of the Cu-*o*-Va complex around +1.10 V, and the reversible process related to the Cu(II)/Cu(I) couple are clearly observed in the CV (Fig. 5.a). The same behavior can be observed in the second scan performed, starting the experiment through the cathodic direction (Figure SI6), indicating that it is necessary to oxidize first the Cu-*o*-Va complex to appreciate the reversible process assigned to Cu/II)/Cu(I) couple. It is remarkable that in this experiment, the contour plots registered in normal (Fig. 5.b) and parallel (Fig. 5.c) configuration provide exactly the same information, indicating that the two processes take place in solution. The main difference in both plots is the net absorbance values obtained in the two configurations. Absorbance values are higher in parallel arrangement than in normal arrangement because of the difference in the two optical pathways.

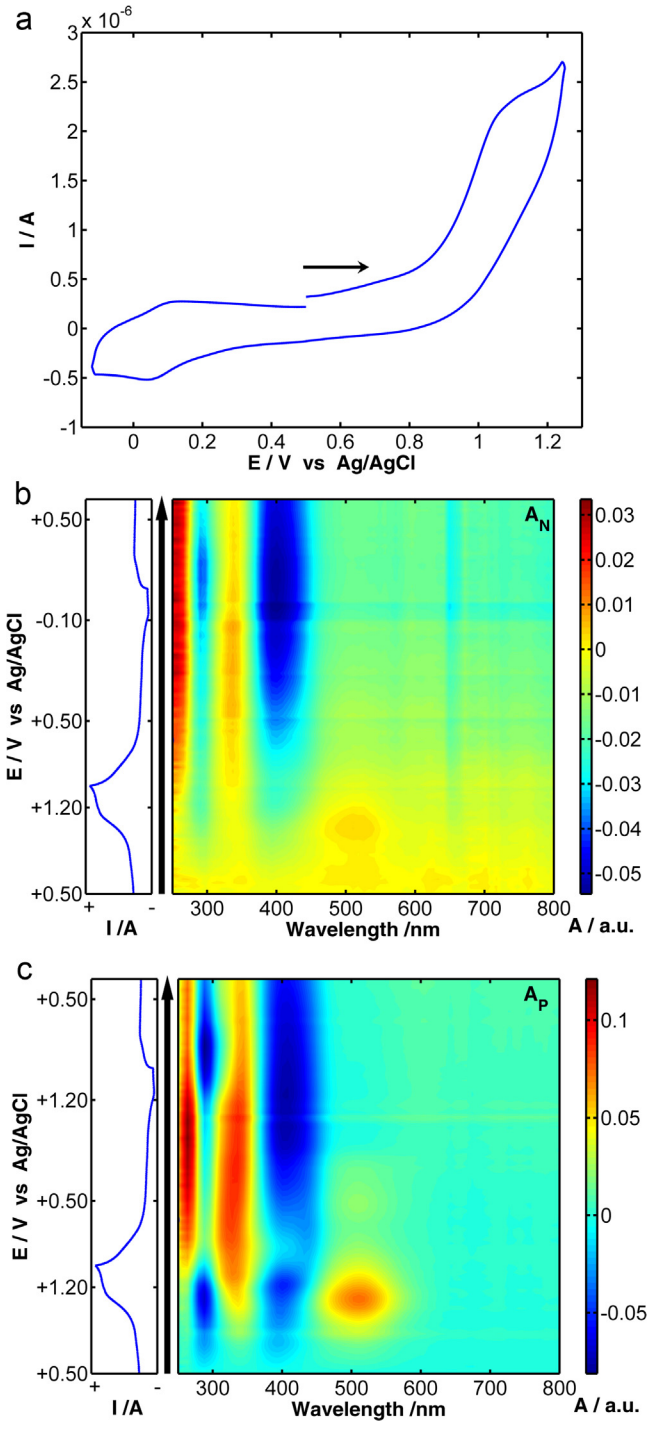

Fig. 5. (a) Cyclic voltammogram and contour plots of absorbance evolution with time (potential) in (b) normal and (c) parallel configuration. For a better understanding of the contour plots, the corresponding 3D plots of absorbance evolution with potential are shown in the supporting info, Figures SI5. One potential cycle from +0.50 V to +1.25 V and back to −0.10 V, ending the experiment at +0.50 V, scanning the potential at 0.005 V s^{-1}. Experiment performed in 10^{-4} M Cu-*o*-Va and 0.1 M $TBAPF_6$ DMSO solution.

Cu-*o*-Va complex is oxidized around +1.10 V, emerging a band around 510 nm related to this oxidation process. This band decreases in the backward scan due to a charge redistribution within the complex because no electrochemical changes are observed in the CV between +1.00 V and +0.40 V. In this potential region, the evolution of three different absorption bands is observed, one decreasing centered at 415 nm and another two increasing at 270 nm and 340 nm. These three absorption bands have to be ascribed to the chemical generation of the new Cu(II) complex that is next reduced to Cu(I) around +0.06 V, as indicated the CV (Fig. 5.a). This last electrochemical process can be observed spectroscopically at 285 nm (Figs. 5.b and 5.c). This band decreases during the reduction of Cu(II) to Cu(I) and increases reversibly at the end of the scan when the initial potential is reached. Therefore, it can be undoubtedly assigned to this reversible process. Moreover, a last BSEC experiment was carried out right after the experiment showed in Fig. 5. In this case a cyclic voltammetry between +0.30 V and −0.10 V at 0.005 V s^{-1} was performed. The comparison between the CV and the DCVA at 285 nm (Fig. 6) evidences that both signals are related exactly with the same process, in this case, the reversible reduction of Cu(II)/Cu(I) complex.

The most intriguing point of these results is related to the new complex generated in solution. As it was explained above, changes in the spectra can be ascribed to a shifting of the position of the absorption bands of the complex during the oxidation process and the subsequent chemical reaction. A first hypothesis was related to the dissociation of the Cu-*o*-Va complex to generate a new copper complex only with solvent molecules as ligands. To study this hypothesis, a spectroelectrochemical experiment was performed in a DMSO solution with 10^{-4} M Cu^{2+} and 0.1 M $TBAPF_6$, scanning the potential between +0.30 and −0.10 V at 0.005 V s^{-1}. Figure SI7 compares the contour plots in parallel configuration of this experiment (Figure SI7.a) with that performed under exactly the same experimental conditions with the oxidized Cu-*o*-Va complex (Figure SI7.b). From these results we can concluded that in both cases the Cu(II)/Cu(I) reversible reduction takes place. However, this reaction does not occur in the same spectral region. While the Cu^{2+} DMSO solution has an absorption band at 305 nm (Figure SI7. a), the new complex shows a band at 285 nm (Figure SI7.b) related to this reduction. Therefore, the dissociation of the Cu-*o*-Va complex should be discarded. In an attempt to identify the new complex formed during the oxidation, an exhaustive electrolysis of a Cu-*o*-Va solution was performed, applying a potential of +1.75 V during 600 s at 150 μL of DMSO solution 0.013 M Cu-*o*-Va and 0.1 M $TBAPF_6$. Next, the reaction product of this electrolysis was analysed by mass spectrometry (Figure SI8). All the samples yield a mass corresponding to the *o*-Va ligand, without mass modification.

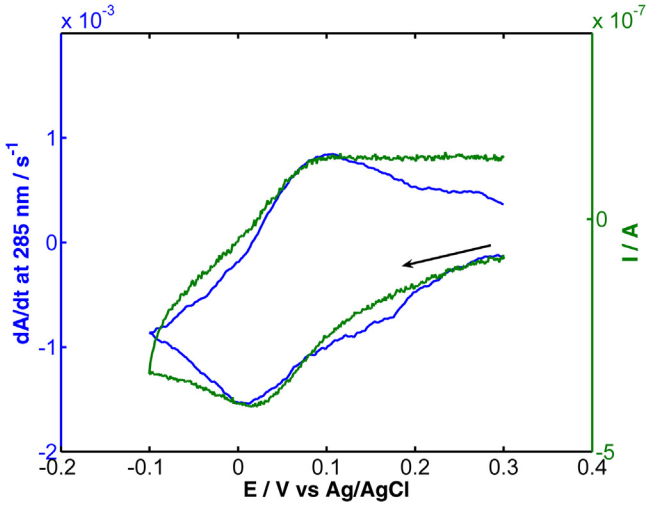

Fig. 6. Cyclic voltammogram (green line) and derivative voltabsorptogram in parallel configuration (blue line). Potential was scanned from + 0.30 V to −0.10 V at 0.005 V s^{-1} in 10^{-4} M Cu-*o*-Va in 0.1 M $TBAPF_6$ DMSO solution.

Therefore, and taking into account that the copper metallic centre is not free after the irreversible Cu-*o*-Va oxidation, as it has been deduced from BSEC experiments, and considering that the ligand of the oxidized Cu-*o*-Va has not suffered any decomposition, as has been inferred from the mass spectrometry data, we have to assume that oxidized *o*-Va is still acting as ligand in the new complex. The shifting of the absorption bands related to this process suggests changes and, consequently, a reorganization of the complex structure after its irreversible oxidation. The new complex acquires a new configuration that favours the electrogeneration of the Cu(I) complex, which is not possible from the pristine Cu-*o*-Va complex. A scheme of the electrochemical reaction involving the complex species is shown in the Supporting Information, Scheme S1.

TDDFT calculations of the suggested products of the electrochemical reactions were carried out to aid in the assignment of the band that evolves in the absorption spectra, thus shedding more light on the mechanism of those reactions.

The calculated and experimental electronic spectra of Cu-*o*-Va in DMSO have been previously compared [30]. Experimental spectrum exhibits four absorption bands that were assigned with the help of the calculations. The ones centered at 266 nm and 410 nm are assigned to intra-ligand transition, whereas the band with maximum at 338 nm is assigned to a charge transfer ligand-to-metal transition. The much less intense band at 712 nm is due to the characteristic *d-d* transition in the complex The concentrations employed in the BSEC experiments are much lower than needed to follow the evolution of this last band.

Calculations, including geometry optimization, have been carried out for the oxidized and reduced complex species. Electronic spectra were calculated in both cases considering the redox process with no change in the original geometry of the pristine complex and also considering the optimized geometry. The redox processes can be analyzed in two steps; the first involving the electron transfer at fixed geometry and the second considering the relaxation of the geometry.

In the oxidation process slight changes of geometry are predicted after relaxation of the system. Nevertheless, as a consequence of changes in the charge distribution of the oxidized ligands, some spectral changes were observed in the calculated spectra. In Figure SI9 spectra of the initial complex and oxidized complexes considering both fixed and optimized geometry are compared. It can be observed that a new band appears in the electron transfer step at approximately 417 nm (oscillator strength of 0.0922). After relaxation of the geometry, that band shifts to 438 nm, but its intensity decreases more than 6 times, its oscillator strength being 0.0151. This fact can explain the behavior of the experimental signal at 415 nm. Molecular orbitals (MO) involved in those transitions are mainly located at the phenolic oxygen atoms and the copper ion, with minor contributions from oxygen atoms of HC=O groups and carbon atoms belonging to the rings. This could be described as a L + M → L transition.

According to the experimental observations during the whole process, absorbance at 340 nm and at 270 nm continuously increases. Interestingly, calculated spectrum of oxidized, fixed-geometry complex shows a band around 330 nm (oscillator strength of 0.1589), which remains almost at the same position, 336 nm, after geometry relaxation, but exhibiting a considerably larger oscillator strength of 0.2617. Also, three calculated transitions around 290 nm are found for the oxidized species at fixed geometry (oscillator strengths of 0.0296, 0.0285 and 0.0266,

respectively). On the other hand, a dominating transition at 251 nm is found when the geometry of the complex is optimized. This transition presents larger oscillator strength of 0.4980. However, it should be noted that it is predicted at a lower wavelength than the solvent cut-off, which occurs at 260 nm, thus it would be absent in the experimental spectrum. The MO's involved in those transitions are mainly located both on the phenolic oxygen atoms and on the aromatic rings, with minor contributions from the HC=O groups. The transitions could be described as L → L ones.

Regarding the reduced species, the optimized geometry for the Cu(I) complex significantly differs from the initial one, with a distorted tetrahedral environment around the copper ion. This structural change is probably slower than the electrochemical process. The absorption spectrum calculated when the geometry of the complex remains fixed shows a strong absorption around 250 nm with a shoulder at 283 nm, see Figure. SI10. That shoulder shifts to 254 nm when the complex geometry becomes optimized, a wavelength that is lower than the solvent cut-off of 260 nm. These findings are consistent with the observed behavior of the experimental band at 285 nm. The MO's involved in the transitions at 283 nm and 254 nm for fixed-geometry complex and optimized-geometry complex, respectively, are located at the phenolic oxygen atoms and the copper ion and are delocalized on the aromatic rings, giving place to a L + M → L transition. Calculated transitions around 250 nm involve MO's that are mainly delocalized on the aromatic rings. These transitions could be described as L → L transitions.

4. Conclusions

A new bidimensional spectroelectrochemistry device has been developed. BSEC has demonstrated to be highly useful to unravel the electrochemical mechanism of oxidation/reduction of Cu(o-Va)$_2$(H_2O)$_2$. This multiresponse technique has provided compelling information related to processes taking place both in solution and on the electrode surface. Summarizing, Cu-*o*-Va complex cannot be directly reduced to Cu(I) complex. This reduction reaction involves the electrodeposition of Cu(0) on the electrode surface. On the other hand, oxidation of Cu-*o*-Va implies oxidation of the *o*-Va ligand, yielding a new Cu(II) complex that suffers some kind of structural change respect to the pristine Cu-*o*-Va. Once this new Cu(II)-*o*-Va complex has been generated, the reversible reduction Cu(II)/Cu(I) occurs. The new device should be a significant advance in spectroelectrochemistry that could lead to new and interesting future applications, particularly, those in which adsorption and/or crystallization processes take place.

Acknowledgments

Support from CONICET, UNLP, Junta de Castilla y León (BU033U16), and Ministerio de Economía y Competitividad (CTQ2014-55583-R, CTQ2014-61914-EXP, CTQ2015-71955-REDT) is gratefully acknowledged. The authors acknowledge Universidad Nacional de Catamarca, Argentina, for computing time and the use of the Gaussian 09 program.

Appendix A. Supplementary data

Supplementary data associated with this article can be found, in the online version, at http://dx.doi.org/10.1016/j.electacta.2017.05.105

References

[1] R.L. Wang, K.Y. Tam, R.G. Compton, Applications of the channel flow cell for UV-visible spectroelectrochemical studies Part 3. Do radical cations and anions have similar diffusion coefficients to their neutral parent molecules? J. Electroanal. Chem 434 (1997) 105–114.
[2] M. Marcaccio, F. Paolucci, C. Paradisi, S. Roffia, C. Fontanesi, L.J. Yellowlees, S. Serroni, S. Campagna, G. Denti, V. Balzani, Electrochemistry of Multicomponent Systems. Redox Series Comprising up to 26 Reversible Reduction Processes in Polynuclear Ruthenium(II) Bipyridine-Type Complexes, J. Am. Chem. Soc. 121 (1999).
[3] M. Marcaccio, F. Paolucci, C. Fontanesi, G. Fioravanti, S. Zanarini, Electrochemistry and spectroelectrochemistry of polypyridine ligands: A theoretical approach, Inorganica Chim. Acta. 360 (2007) 1154–1162.
[4] I. Gallardo, G. Guirado, J. Marquet, N. Vilà, Evidence for a π Dimer in the Electrochemical Reduction of 1,3,5-Trinitrobenzene: A Reversible N2-Fixation System, Angew. Chemie Int. Ed. 46 (2007) 1321–1325.
[5] R.O. Al-Kaysi, J.L. Bourdelande, I. Gallardo, G. Guirado, J. Hernando, Investigation of an Acid-Base and Redox Molecular Switch: From Bulk to the Single-Molecule Level, Chem. – A Eur. J. 13 (2007) 7066–7074.
[6] W. Kaim, J. Fiedler, Spectroelectrochemistry: the best of two worlds, Chem. Soc. Rev. 38 (2009) 3373–3382.
[7] T. Kuwana, R.K. Darlington, D.W. Leedy, Electrochemical Studies Using Conducting Glass Indicator Electrodes, Anal. Chem. 36 (1964) 2023–2025.
[8] B. Ren, X.-B. Lian, Jian-Feng Li, P.-P. Fang, Q.-P. Lai, Z.-Q. Tian, Spectroelectrochemical flow cell with temperature control for investigation of electrocatalytic systems with surface-enhanced Raman spectroscopy, Faraday Discuss. 140 (2008) 155–165.
[9] D. Ibañez, C. Fernández-blanco, A. Heras, Á. Colina, Time-Resolved Study of the Surface-Enhanced Raman Scattering E ff ect of Silver Nanoparticles Generated in Voltammetry Experiments, J. Phys. Chem. C. 118 (2014) 23426–23433.
[10] J. Zeitouny, V. Jouikov, Reversed redox generation of silyl radicals in a four-electrode flow-through EPR spectroelectrochemical cell, Phys. Chem. Chem. Phys. 11 (2009) 7161–7170.
[11] S. Klod, F. Ziegs, L. Dunsch, In situ NMR spectroelectrochemistry of higher sensitivity by large scale electrodes, Anal. Chem. 81 (2009) 10262–10267.
[12] P.R. Murray, D. Collison, S. Daff, N. Austin, R. Edge, B.W. Flynn, L. Jack, F. Leroux, E.J.L. McInnes, A.F. Murray, D. Sells, T. Stevenson, J. Wolowska, L.J. Yellowlees, An in situ electrochemical cell for Q- and W-band EPR spectroscopy, J. Magn. Reson. 213 (2011) 206–209.
[13] H. Visser, A.E. Curtright, J.K. McCusker, K. Sauer, Attenuated total reflection design for in situ FT-IR spectroelectrochemical studies, Anal. Chem. 73 (2001) 4374–4378.
[14] C.M. Burba, R. Frech, In situ transmission FTIR spectroelectrochemistry: A new technique for studying lithium batteries, Electrochim. Acta. 52 (2006) 780–785.
[15] I.S. Zavarine, C.P. Kubiak, A versatile variable temperature thin layer reflectance spectroelectrochemical cell, J. Electroanal. Chem. 495 (2001) 106–109.
[16] E. Muñoz, Á. Colina,, A. Heras, V. Ruiz, S. Palmero, J. López-Palacios, Electropolymerization and characterization of polyaniline films using a spectroelectrochemical flow cell, Anal. Chim. Acta 573–574 (2006) 20–25.
[17] A. Heras, A. Colina, V. Ruiz, J. López-Palacios, UV-Visible Spectroelectrochemical Detection of Side-Reactions in the Hexacyanoferrate (III)/(II) Electrode Process, Electroanalysis 15 (2003) 702–708.
[18] D. Izquierdo, A. Martinez, A. Heras, J. López-Palacios, V. Ruiz, R.A.W. Dryfe, Á. Colina, Spatial scanning spectroelectrochemistry. Study of the electrodeposition of Pd nanoparticles at the liquid/liquid interface, Anal. Chem. 84 (2012) 5723–5730.
[19] H. Isago, A new spectroelectrochemical cell with a long optical path length for redox studies of phthalocyanines, J. Porphyr. Phthalocyanines. 10 (2006) 1125–1131.
[20] P.A. Flowers, J.C. Strickland, Easily Constructed Microscale Spectroelectrochemical Cell, Spectrosc. Lett. 43 (2010) 528–533.
[21] S. Haymond, J.K. Zak, Y. Show, J.E. Butler, G.T. Babcock, G.M. Swain, Spectroelectrochemical responsiveness of a freestanding boron-doped diamond, optically transparent electrode toward ferrocene, Anal. Chim. Acta. 500 (2003) 137–144.
[22] P.A. Flowers, D.A. Blake, Submicroliter electrochemistry and spectroelectrochemistry using standard electrodes and a polymer electrolyte salt bridge, Anal. Chem. 85 (2013) 3059–3063.
[23] G. Seshadri, H. Mo, J.A. Kelber, Spectroelectrochemical Studies of Nickel Oxidation in Aerated Phosphate Solutions, Lagmuir. 16 (2000) 6037–6042.
[24] J.L. Anderson, Circulating long-optical-path, thin-layer electrochemical cell for spectroelectrochemical characterization of redox enzymes, Anal. Chem. 51 (1979) 2312–2315.
[25] M. Velický, K.Y. Tam, R.A.W. Dryfe, Permeation of a fully ionized species across a polarized supported liquid membrane, Anal. Chem. 84 (2012) 2541.
[26] J. López-Palacios, Á. Colina,, A. Heras, V. Ruiz, L. Fuente, Bidimensional spectroelectrochemistry, Anal. Chem 73 (2001) 2883–2889.
[27] J. Garoz-Ruiz, A. Heras, S. Palmero, A. Colina, Development of a Novel Bidimensional Spectroelectrochemistry Cell Using Transfer Single-Walled Carbon Nanotubes Films as Optically Transparent Electrodes, Anal. Chem. 87 (2015) 6233–6239.
[28] T. Kuwana, J.W. Strojek, Kinetic and mechanism studies of o-tolidine electro-oxidation using optically transparent electrodes, Discuss. Faraday Soc. 45 (1968) 134–144.
[29] O. Orcajo, E. Ventosa, A. Martínez, Á. Colina,, A. Heras, V. Ruiz, J. López-Palacios, A new reflection-transmission bidimensional spectroelectrochemistry cell:

Electrically controlled release of chemicals from a conducting polymer, J. Electroanal. Chem 596 (2006) 95–100.
[30] A.C. González-Baró, R. Pis-Diez, C.A. Franca, M.H. Torre, B.S. Parajón-Costa, Physicochemical characterization of Cu(II) complexes with SOD-like activity, theoretical studies and biological assays, Polyhedron. 29 (2010) 959–968.
[31] M. Odabağlu, F. Arslan, H. Ölmez, O. Büyükgüngör, Synthesis, crystal structures and spectral characterization of trans-bisaquabis(*o*-vanillinato)copper(II), cis-aquabis(*o*-vanillinato)copper(II) and aqua[bis(*o*-vanillinato)-1, 2-ethylenediimin]copper(II), Dye. Pigment. 75 (2007) 507–515.
[32] C. Zhang, S.-M. Park, In Situ Spectroelectrochemical Studies on the Anodic Oxidation of Nickel Hydroxide in Alkaline Media, J. Electrochem. Soc. 136 (1989) 3333–3342.
[33] N. González-Diéguez, Á. Colina,, J. López-Palacios, A. Heras, Spectroelectrochemistry at screen-printed electrodes: Determination of dopamine, Anal. Chem 84 (2012) 9146–9153.
[34] A.D. Becke, Density-functional thermochemistry. III. The role of exact exchange, J. Chem. Phys. 98 (1993) 5648–5652.
[35] C. Lee, W. Yang, R.G. Parr, Development of the Colle-Salvetti correlation-energy formula into a functional of the electron density, Phys. Rev. B. 37 (1988) 785–789.
[36] T.H. Dunning Jr., Gaussian basis sets for use in correlated molecular calculations. I. The atoms boron through neon and hydrogen, J. Chem. Phys. 90 (1989) 1007–1023.
[37] R.a. Kendall, T.H. Dunning Jr., R.J. Harrison, Electron affinities of the first-row atoms revisited. Systematic basis sets and wave functions, J. Chem. Phys. 96 (1992) 6796–6806.
[38] D. Figgen, G. Rauhut, M. Dolg, H. Stoll, Energy-consistent pseudopotentials for group 11 and 12 atoms: Adjustment to multi-configuration Dirac-Hartree-Fock data, Chem. Phys. 311 (2005) 227–244.
[39] K.A. Peterson, C. Puzzarini, Systematically convergent basis sets for transition metals. II. Pseudopotential-based correlation consistent basis sets for the group 11 (Cu, Ag Au) and 12 (Zn, Cd, Hg) elements, Theor. Chem. Acc. 114 (2005) 283–296.
[40] S. Miertuš, E. Scrocco, J. Tomasi, Electrostatic interaction of a solute with a continuum. A direct utilizaion of AB initio molecular potentials for the prevision of solvent effects, Chem. Phys. 55 (1981) 117–129.
[41] S. Miertus, J. Tomasi, Approximate evaluations of the electrostatic free energy and internal energy changes in solution processes, Chem. Phys. 65 (1982) 239–245.
[42] M.E. Casida, C. Jamorski, K.C. Casida, D.R. Salahub, Molecular excitation energies to high-lying bound states from time-dependent density-functional response theory: Characterization and correction of the time-dependent local density approximation ionization threshold, J. Chem. Phys. 108 (1998) 4439–4449.
[43] M.J. Frisch, G.W. Trucks, H.B. Schlegel, G.E. Scuseria, M.A. Robb, J.R. Cheeseman, G. Scalmani, V. Barone, B. Mennucci, G.A. Petersson, H. Nakatsuji, M. Caricato, X. Li, H.P. Hratchian, A.F. Izmaylov, J. Bloino, G. Zheng, J.L. Sonnenberg, M. Hada, M. Ehara, K. Toyota, R. Fukuda, J. Hasegawa, M. Ishida, T. Nakajima, Y. Honda, O. Kitao, H. Nakai, T. Vreven, J.A. Montgomery Jr., J.E. Peralta, F. Ogliaro, M. Bearpark, J.J. Heyd, E. Brothers, K.N. Kudin, V.N. Staroverov, T. Keith, R. Kobayashi, J. Normand, K. Raghavachari, A. Rendell, J.C. Burant, S.S. Iyengar, J. Tomasi, M. Cossi, N. Rega, J.M. Millam, M. Klene, J.E. Knox, J.B. Cross, V. Bakken, C. Adamo, J. Jaramillo, R. Gomperts, R.E. Stratmann, O. Yazyev, A.J. Austin, R. Cammi, C. Pomelli, J.W. Ochterski, R.L. Martin, K. Morokuma, V.G. Zakrzewski, G.A. Voth, P. Salvador, J.J. Dannenberg, S. Dapprich, A.D. Daniels, O. Farkas, J.B. Foresman, J.V. Ortiz, J. Cioslowski, D.J. Fox, Gaussian 09, Revision B.01, Gaussian, Inc, Wallingford, CT, 2010.
[44] J. López-Palacios, Á. Colina, A. Heras, V. Ruiz, L. Fuente, Á. Colina, A. Heras, V. Ruiz, L. Fuente, Bidimensional spectroelectrochemistry, Anal. Chem 73 (2001) 2883–2889.
[45] Q. Li, C. Batchelor-McAuley, R.G. Compton, Electrooxidative decarboxylation of vanillylmandelic acid: voltammetric differentiation between the structurally related compounds homovanillic acid and vanillylmandelic acid, J. Phys. Chem. B 114 (2010) 9713–9719.